Applied Mathematical Modelling 115 (2023) 398–413

Contents lists available at ScienceDirect

Applied Mathematical Modelling

journal homepage: www.elsevier.com/locate/apm

Mathematical modeling of heterogeneous metal foams for phase-change heat transfer enhancement of latent heat thermal energy storage units

Mehdi Ghalambaz [a], Mutabe Aljaghtham [b], Ali J. Chamkha [c], Abdelkader Abdullah [b,d], Ibrahim Mansir [b,e], Mohammad Ghalambaz [f,*]

[a] Institute of Research and Development, Duy Tan University, Da Nang 550000, Viet Nam
[b] Mechanical Engineering Department, College of Engineering in Al-Kharj, Prince Sattam Bin Abdulaziz University, Al-Kharj 11942, Saudi Arabia
[c] Faculty of Engineering, Kuwait College of Science and Technology, Doha, Kuwait
[d] Mechanical Power Engineering Department, Faculty of Engineering, Tanta University, Tanta 31521, Egypt
[e] Centre for Energy Research and Training, Ahmadu Bello University, P.M.B 1045, Zaria, Nigeria
[f] Department of Theoretical Mechanics, Tomsk State University, 36 Lenin Ave., Tomsk 634050, Russia

ARTICLE INFO

Article history:
Received 12 August 2022
Revised 25 September 2022
Accepted 10 October 2022
Available online 14 October 2022

Keywords:
Heterogeneous metal foam
Latent heat thermal energy storage
Melting heat transfer
Anisotropic porous media

ABSTRACT

Embedding phase change material in metal foams improves the heat transfer characteristics of a thermal energy storage device. Here, the melting heat transfer of phase change materials embedded in a heterogeneous metal foam was addressed in a cavity heated from a side wall. The heterogeneity of the metal foam can be controlled through a heterogeneity parameter and heterogeneity angle. The thermal conductivity and permeability of the metal foam were introduced by tensors. The governing equations for the natural convection flow and phase change heat transfer, including anisotropic thermal conductivity and permeability, were introduced and solved by the finite element method. The impact of the heterogeneity parameter and angle on the melting time and isotherm and streamline patterns were investigated. The results showed an increase in heterogeneity could increase the heat transfer rate and shorten the melting time. A heterogeneity angle significantly changes the melting (thermal charging time) by 24% when the heterogeneity parameter was 0.2. Depending on the heterogeneity angle, the melting time could be significantly shortened or extended compared to a simple metal foam. For a fixed weight of foam, a heterogeneous metal foam could shorten the charging time by 11% compared to a simple foam.

© 2022 Elsevier Inc. All rights reserved.

1. Introduction

The field of energy has become one of the most crucial research areas in recent decades. Governments are increasingly concerned about global warming and greenhouse gas emissions, which has led to a shift toward a more sustainable and renewable energy source. The problem with renewable energy is that it is unpredictable, often unavailability, and has variable outputs; therefore, demand does not match supply. TES (thermal energy storage) could help bridge the gap between

* Corresponding author.
E-mail addresses: mehdighalambaz@duytan.edu.vn (M. Ghalambaz), m.ghalambaz@gmail.com (M. Ghalambaz).

https://doi.org/10.1016/j.apm.2022.10.018
0307-904X/© 2022 Elsevier Inc. All rights reserved.

demand and supply [1]. There are generally three kinds of TES systems: chemical, sensible, and latent heat (LHS) [2]. The LHS systems are more popular than the other two due to their practically constant operating temperatures and high energy density. The heat is absorbed and released through the phase change process in these energy storages. It means the ability of PCMs (phase change materials) to transfer heat is critical for the efficiency of the LHS unit. As an organic PCM, paraffin can store large amounts of energy under low-temperature variations [3]. Paraffin is non-toxic, and exhibits excellent stability. Even so, one of its disadvantages is its low thermal conductivity. PCM's thermal conductivity can be increased by various additives, e.g., nanoparticles [4], fins [5–7], encapsulation of the PCM [8], and graphene matrix [9].

Another possibility is to use MF (metal foam), which consists of several metallic ligaments connected, and in which different cells may be distinguished by pore separation [10,11]. These foams are known for their light weight, thermal conductivity, tortuosity, and high surface-area-to-volume ratio for heat transfer applications like solar receivers [12], heat sinks [13], and TES systems [14]. For the effective increase in PCM conductivity and providing appropriate composites, MFs are a suitable additive since they are less expensive than additives such as graphene and carbon nanotube. Recent developments have resulted in the development of thin-film MFPCM systems for cooling various electronic components, including GPUs, CPUs, laptops, LCDs, and tablets [15]. The present study employed the foam structure due to its mentioned advantages.

Nie et al. [16] investigated how foams made from copper affected the thermal cycle of paraffin. It has been demonstrated that MF has enhanced heat transfer and phase changes. Further, Zhang et al. [17] reported that using copper foam could reduce the total melting time of paraffin by 20.5%. Razack [18] developed MFPCM batteries that work at a lower temperature and produce more power; this new battery technology can generate more energy and extend the battery's lifespan. Guo et al. [19] used a compressed metal foam for thermal energy storage, which saved the melting time by 13.9% compared to same MF with no compression. Liu et al. [20] used several layers of metal foam with different porosities in a vertical shell-tube shape LHTES unit. An optimal arrangement of MF layers could shorten the charging/discharging time by 10.9%. Deng et al. [21] developed and verified a model of melting heat transfer in fractal porous foam. The model was used to investigate the impact of pore distribution of the melting heat transfer. The results showed the melting process was influenced by fractal dimension even for a similar porosity. In another study, Xu et al. [22] utilized a fractal model and showed the pore distribution can affect the phase change process.

Sabrina Ferfera et al. [23] investigated the porosity of porous composites and discovered that lower porosity results in higher thermal conductivities, whereas tiny pores result in uniform melting fronts within a composite. In addition, to appreciate thermal conductivity augmentation, Tauseef ur et al. [24] summarized the effects of MFs on PCMs. In a hyper-gravity environment, Filippeschi et al. [25] evaluated the impact of convection on the melting of aluminum foam and paraffin wax composite material. According to the experiments, hyper-gravity accelerates melting by 12%. The experiments show a convection regime that accelerates the phase change process. Hu et al. [26] used numerical analysis to analyze MFPCM's contact and thermal conditions. In their research, the connection between the heated wall and metal foam did not significantly affect top heating; however, it involved melting under left wall heating.

An MF's fractal dimensions, in addition to its porosity, significantly affect the TES performance. The MF with a smaller fractal dimension might provide a better phase change rate; however, the discontinuous melting caused by the MF may negatively impact the system's performance [21]. Experimental analysis of different inclination angles of the TES demonstrated that the MF suppresses natural convection [27]. In the TES system, the MF significantly affects the heat transfer rate. Heat transfer in MFs is known to be affected by anisotropy [28]. Thus, its structure could also play an important role. An anisotropy could be induced by manufacturers and might be induced with the help of modern techniques like additive manufacturing [29,30].

Gravity, compression, and viscous forces cause anisotropy in conductivity in MFs embedded with PCM [31]. Several approaches have been proposed and presented to resolve the challenges mentioned in this respect. Zhu et al. [32] inserted a fin at the bottom of an MFPCM with graded porosity and evaluated the porosity grade and fin thickness impacts. According to reports, the presence of fins modified the melting sequence, and graded foams boosted the heat transfer rate. Joshi and Rathod [33] examined the implications of the optimal placement of MF in the PCM, concluding that MF placed at higher gradients of temperature could lead to better heat transfer. So, an appropriately placed MF would be capable of reducing its adverse impact on heat convection while also minimizing the TES's additional costs. The utilization of multi-segment MFs with varying porosity demonstrated that the cascaded foams resulted in more uniform temperatures, thereby reducing the rate of phase change [34].

The use of multiple PCMs and MFs segments reduced the solidification time by up to 94% compared with a non-enhanced case [35]. Xu et al. [36] performed a numerical investigation to identify the optimal properties of distinct foam layers. To balance phase-change performance and material cost, they compared three cases: 1/3, 0.72, and 1 of a foam made of copper with a pure PCM. If the price of considered foam were five times greater than that of PCM, the case with a 1/3 filling ratio would have the highest phase change rate for a given material cost.

Iasiello et al. [37] performed numerical analyses on thermal conductivity in MFs with various porosities, finding that cell elongation is related to the thermal conductivity of the foam [38]. Furthermore, they presented experimental and numerical results for aluminum foams coupled with PCM under various MF's porosity, temperatures, orientations, and pore sizes (PPIs) [39]. A decrease in porosity drastically reduces melting time, whereas PPI is irrelevant, and minor effects are apparent in orientation. For a foam with a porosity of 0.94, Amani et al. reported similar results [40]. Vijay et al. [41] performed a computed tomography and geometrically characterized the actual MF structures. They found that the inlet flow direction impacted heat transfer rates due to the foam's anisotropy. A numerical study of the effects of pore density and average

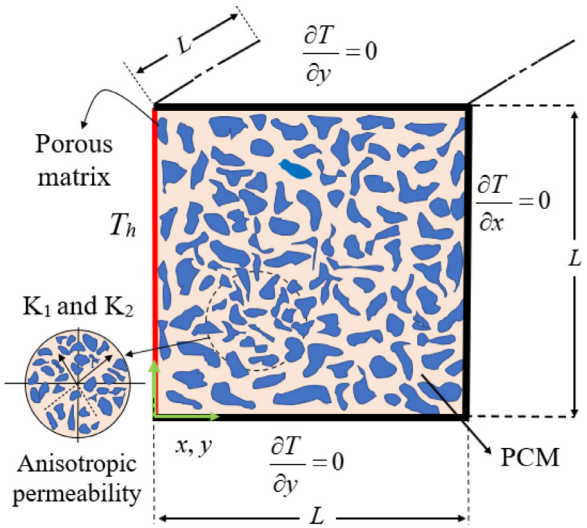

Fig. 1. Schematic view of the physical model. The thermal conductivity and permeability are anisotropic.

porosity was conducted by Yang et al. [42] to investigate MFs with non-uniform porosity. Increasing porosity from bottom to top reduces the melting rate due to enhanced natural convection. Huang et al. [43] demonstrated in an experiment and numerical study that the melting rate of the PCM accelerated as the porosity of the MF decreased.

Bamdezh et al. [44] developed a thermal management system and studied the effect of MF anisotropy on the system's performance. The findings show that simply raising the tangential conductance increases the melting rate and average cell temperature. Furthermore, rising axial heat conductivity has a good impact on reducing cell temperature differentials. Yu et al. [45] studied the anisotropic properties of two kinds of pore geometries. It was evident from this study that when using metal foams, it is essential to consider the influence of anisotropic characteristics. Ren et al. [46] explored the anisotropic thermal conduction in a woven MFPCM composite, which showed clear benefits over isotropic porous media in enhancing the thermal performance of a TES unit. It concluded that designing anisotropic woven MF in the desired direction would significantly increase the performance and reduce the cost.

The literature review revealed that the studies on the thermal advantage of anisotropic metal foams for energy storage systems are scarce. The current study looks at the effect of MF anisotropy on the heat transfer performance of a latent heat energy storage system for the first time.

2. Model description and mathematical formulation

Fig. 1 shows a schematic of a physics model with dimensions and boundary conditions. As can be seen, a closed cubic-square chamber with dimensions L × L, saturated with a porous medium and phasing material, is intended for the storage of thermal energy. The porous medium is anisotropic and at certain angles. Thus, the thermal conductivity and permeability are not identical in different directions. The phase change material and the porous solid matrix are in local thermal equilibrium (LTE) at all times.

In some thermal energy storage applications for waste heat recovery and solar systems, a working heat transfer fluid (HTF) flows inside the LHTES unit and exchanges heat to the PCM through a wall. In such applications, the boundary condition is the convective heat transfer at the wall (boundary). Increasing the flow rate at the HTF side increases the convective heat transfer strength, and the wall temperature asymptotically reaches the HTF temperature, representing the constant wall temperature boundary condition. Here, it was assumed that the HTF side is heating the storage unit with its maximum power; thus, the isotherm boundary condition is adopted for the heated wall. Thus, the left wall is at a high isothermal temperatures and other walls are insulated. After a short time and with the melting conditions provided, the melting front will be formed near the hot wall on the left and will advance over time.

The melting front under the influence of an anisotropic porous environment can have more or less progress, or the interface line can have a noticeable deformation. Also, any slippage of the molten phase change material in the vicinity of the chamber walls is avoided. There is a smooth flow and natural heat transfer mode in the chamber. In addition, the phase change material is incompressible with a Newtonian behavior. The Boussinesq approximation is used for density changes.

Typically, some temperature differences between the MF and PCM inside the pores could arise in regions where the heat source is closer or where there is the solid/liquid boundary [47,48]. This effect can be captured using a local thermal non-equilibrium model. However, some empirical investigation [49] report that the local thermal non-equilibrium (LTNE) condition could be significant solely at the beginning of the phase change where the melting interface is next to a heated surface. After that, the local thermal equilibrium (LTE) condition could be reached swiftly. Jiao et al. [50] addressed the LTNE

condition for the paraffin embedded in nickel or copper MF experimentally and theoretically. The results indicated that the temperature variations between the MF and the PCM were evident solely next to a heated wall in the beginning of the melting process. Similarly, a pore-scale study [51] confirms the presence of some LTNE condition in the beginning of the melting process but it fades after a while. Likewise, numerical simulations of [52] using LTNE and LTE conditions reveals that there is a slight difference between the melting fraction curves computed by these models. Thus, the LTE model could be accurate for many thermal energy storage applications, and it was adopted in the present study for the sake of simplicity. The governing equations for the mass, momentum, and energy with phase change can be explained as [53]:

Conservation of mass:

$$\frac{\partial u}{\partial x}+\frac{\partial v}{\partial y}=0 \tag{1}$$

x-momentum:

$$\frac{\rho_p}{\varepsilon}\frac{\partial u}{\partial t}+\frac{\rho_p}{\varepsilon^2}\left(u\frac{\partial u}{\partial x}+v\frac{\partial u}{\partial y}\right)=-\frac{\partial P}{\partial x}+\left(\frac{\partial}{\partial x}\left(\frac{\mu_p}{\varepsilon}\frac{\partial u}{\partial x}\right)+\frac{\partial}{\partial y}\left(\frac{\mu_p}{\varepsilon}\frac{\partial u}{\partial y}\right)\right) -\frac{\mu_p}{\kappa(x,y)}u-s(T).u \tag{2}$$

y-momentum

$$\frac{\rho_p}{\varepsilon}\frac{\partial u}{\partial t}+\frac{\rho_p}{\varepsilon^2}\left(u\frac{\partial v}{\partial x}+v\frac{\partial v}{\partial y}\right)=-\frac{\partial P}{\partial y}+\left(\frac{\partial}{\partial x}\left(\frac{\mu_p}{\varepsilon}\frac{\partial v}{\partial x}\right)+\frac{\partial}{\partial y}\left(\frac{\mu_p}{\varepsilon}\frac{\partial v}{\partial y}\right)\right) -\frac{\mu_p}{\kappa(x,y)}v-s(T).v+\rho_p g\beta_p\left(T-T_f\right) \tag{3}$$

Energy conservation:

$$(\rho c_p)_{\text{eff}}\frac{\partial T}{\partial t}+(\rho c_p)_p\left(u\frac{\partial T}{\partial x}+v\frac{\partial T}{\partial y}\right)+\varepsilon\rho_p L_f\frac{\partial \omega(T)}{\partial t} =\frac{\partial}{\partial x}\left(k_{\text{eff,p}}(x,y)\frac{\partial T}{\partial x}\right)+\frac{\partial}{\partial y}\left(k_{\text{eff,p}}(x,y)\frac{\partial T}{\partial y}\right) \tag{4}$$

where, u and v are the velocities in x and y directions. The temperature field (T) and melt volume fraction (ω) were used in Eq. (4). In the momentum equation, the sink term $s(T)$ was defined as $s(T)=A_{mush}[1-\omega(T)]^2/[\lambda+\omega^3(T)]$, where A_{mush} was taken as a big number (10^{+10} Pa·s/m^2), and λ was a small value (0.001) to prevent division to zero. The sink term s, tends to extremely large magnitudes in solid regions ($\omega\approx0$), which forces the velocities in the momentum equation to zero. Besides, s tends to zero in molten areas($\omega\approx1$) and vanishes from the momentum equation. The gravitational acceleration (g) was considered against the y axis. The subscripts l, s, f, PCM, and eff denote the liquid phase, solid phase, fusion property, phase change material, and effective properties, respectively.

Moreover, x and y are the material coordinates, and t denotes time. The thermophysical properties are the sensible specific heat capacity (C_p), thermal conductivity (k), density (ρ), dynamic viscosity (μ), fusions' latent heat (L_f), and the coefficient of the volumetric thermal expansion (β). The metal foam is characterized by its porosity (ε), thermal conductivity (k_{mf}), and permeability (κ), where the placement of mf in the subscript represent the metal foam property. The metal foam's structure is heterogenous, meaning its permeability and thermal conductivity are different in x and y directions. Supporting the ligaments material in a direction improves the thermal conductivity (more metal to counduct heat) but reduces the permeability (more metal blocks the pore passage). Thus, for a perpendicular coordinate system, the thermal conductivity in directions 1 and 2 are introduced as $k_1=(1+\delta)\times k$ and $k_2=(1-\delta)\times k$, where δ is the amount of the change of thermal conductivity in a direction. As seen, improving thermal conductivity in one direction would reduce it in another direction. Similarly, permeability is introduced likewise to thermal conductivity but in the opposite direction. Thus, the permeability is introduced as $\kappa_1=(1-\delta)\times\kappa$ and $k_2=(1+\delta)\times\kappa$. Here, k and κ indicate metal foam's thermal conductivity and permeability with no heterogeneity.

Now, for the placement of metal foam in an arbitrary direction γ, as depicted in Fig. (1), the matrixes of thermal conductivity and permeability are introduced as:

$$\kappa_{mf}=\begin{bmatrix}\kappa_1(\cos\gamma)^2+\kappa_2(\sin\gamma)^2 & (\kappa_1-\kappa_2)(\sin\gamma)(\cos\gamma)\\ (\kappa_1-\kappa_2)(\sin\gamma)(\cos\gamma) & \kappa_2(\cos\gamma)^2+\kappa_1(\sin\gamma)^2\end{bmatrix} \tag{5a}$$

$$k_{mf}=\begin{bmatrix}k_1(\cos\gamma)^2+k_2(\sin\gamma)^2 & (k_1-k_2)(\sin\gamma)(\cos\gamma)\\ (k_1-k_2)(\sin\gamma)(\cos\gamma) & k_2(\cos\gamma)^2+k_1(\sin\gamma)^2\end{bmatrix} \tag{5b}$$

Here, the fusion temperature range (ΔT_f) was used to describe the liquid fraction (ω) as a function of temperature around the fusion temperature (T_f):

$$\omega(T)=\begin{cases}0 & T<T_f-\Delta T_f/2\\ \dfrac{T-T_f}{\Delta T_f}+\dfrac{1}{2} & T_f-\Delta T_f/2<T<T_f+\Delta T_f/2\\ 1 & T>T_f+\Delta T_f/2\end{cases} \tag{6}$$

Table 1
Thermophysical properties of PCM and copper.

Properties	PCM	Copper foam [17]
μ_l (N.s.m^{-2})	0.006	–
C_p (J.kg^{-1}.K^{-1})	2300	386
k (W.m^{-1}.K^{-1})	0.15	380
h_f (kJ.kg^{-1})	187.2	–
β (K^{-1})	0.0008	–
ρ (kg.m^{-3})	912	8900

where, ΔT_f=5 °C. The heat capacity and thermal conductivity at the mushy region were evaluated as:

$$(\rho C_p) = (1-\phi)(\rho C_p)_{p(s)} + \phi(\rho C_p)_{p(l)} \tag{7a}$$

$$k_p = (1-\phi)k_{(s)} + \phi k_{(l)} \tag{7b}$$

Then, the effective heat capacity and thermal conductivity of composite PCM-metal foam are evaluated using the following equations:

The effective sensible heat capacity of the PCM composite is evaluated as:

$$(\rho C_p)_{\text{eff,p}} = (1-\varepsilon)(\rho C_p)_{mf} + \varepsilon(\rho C_p)_p \tag{9}$$

The effective thermal conductivity of a MF can be computed using various models such as [54–56]. The effective thermal conductivity of composite and PCM was computed using the relation proposed by Bhattacharya et al. [56], which is in excellent agreement with the experimental measurements of [57]:

$$k_{\text{eff}} = A\left(\varepsilon k_{PCM} + (1-\varepsilon)k_{mf}\right) + \frac{1-A}{\left(\frac{\varepsilon}{k_{pcm}} + \frac{1-\varepsilon}{k_{mf}}\right)} \tag{10}$$

where, A=0.35 [56]. In the present formulation, it was assumed that there is a local thermal equilibrium between the metal foam and PCM inside the pores. The natural convection was also taken into account using the Boussinesq approximation. Moreover, the density changes during the phase change were also neglected. The large value of A_{mush} was adopted as 1×10^{10} Pa s/m^2. The value of A_{mush} was increased in the metal foam layer since the flow resistance is high in such a region and demands a larger value of A_{mush}. The pore per inch, ω_p, for metal foam was taken as 20 in the present research. The melting temperature of PCM was considered independent of the metal foam and equal to 46 °C. Moreover, the thermophysical properties of PCM and porous matrix are reported in Table 1.

The zero velocity and permeability boundary conditions were applied to all enclosure walls. Moreover, all walls are well insulated (zero heat flux) except the left side wall, which is at a constant temperature of T_h=70 °C. The PCM and metal foam are initially at a supper cold temperature of T_0=25 °C. The porosity was fixed at ε=0.95 with 10 PPI pore density. The average permeability of MF can be computed using literature models such as [58,59]. Here, the permeability of MF for ε=0.95 was calculated as κ= 9.6536E-8 m^2 using [59].

Finally, the charactrestics parameters are explaned as:

The total melting fraction (MVF) was introduced as:

$$MVF = \frac{\int_A \alpha dA}{\int_A dA} \tag{11}$$

where, since the porosity was fixed it was omitted from the equation. The total stored energy can be computed as summation of the latent and sensible as:

$$\textbf{Totalstoredenergy} = \textbf{sensibleenergy} + \textbf{latentheatenergy} \tag{12}$$

where, $\text{latentheat energy} = \int_A L_f \varepsilon \alpha dA$, and $\text{sensibleenergy} = \int_A (\int_{T_0}^{T} \rho C_p dT) dA$, while the cavity's element was denoted by dA. The melting time (t_{melt}) is considered as the full melting time when MVF>0.995.

3. Numerical method and code verification

3.1. The finite element method

The partial differential equations described in Eqs. (1)–(4) along with the initial and boundary conditions were solved, invoking the finite element method (FEM) [60]. The second-order discretization was adopted for momentum and heat equations after transforming them into a weak form. The Gauss quadrature integration was employed to integrate the equations over elements and obtain an algebraic set of the residual equations. Then, the residual equations were solved iteratively

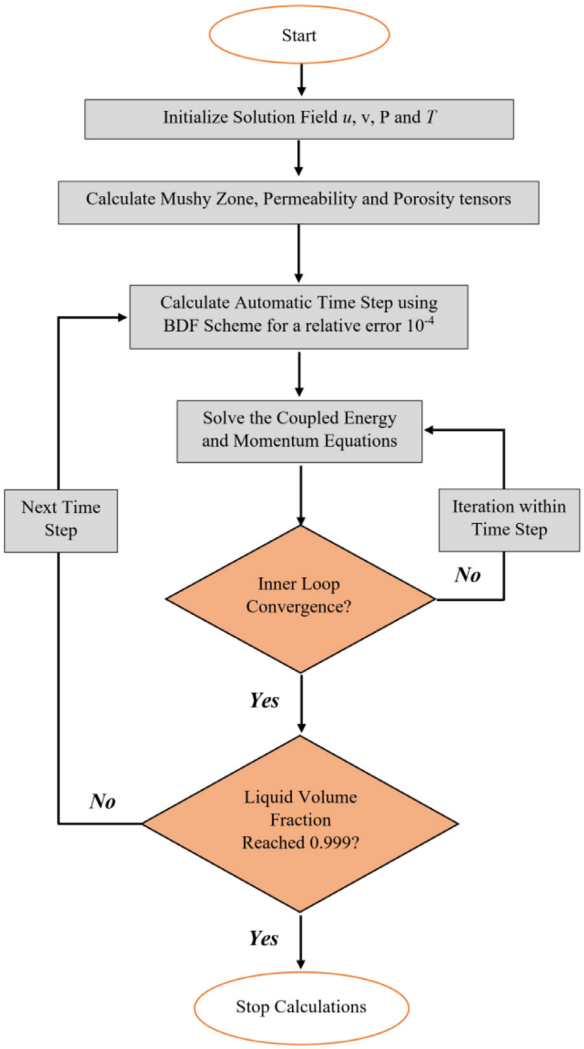

Fig. 2. A diagram of FEM applied for simulation of latent heat thermal energy storage of the phase change material embedded in an open cell heterogeneous metal foam.

using the PARDISO solver in a coupled way by using the Newton method. A damping factor of 0.8 was set to enhance the convergence. The time step was controlled using the backward differential formula [61] with a free order between 1 and 2 to maintain the relative solution accuracy below 10E-4. A diagram of the solution method is depicted in Fig. 2.

3.2. Mesh independency

A uniform structured mesh was employed to discretize the governing equations over the domain of the solution. A highly heterogeneous case with δ=0.3 with a heterogeneous angle γ=45 was selected for the mesh study. The accuracy of the solution with respect to different mesh sizes was investigated by recomputing the results at five different mesh sizes. The mesh size variable (*Mesh* $\times$ *Mesh*) indicates the mesh size. Fig. 3 depicts the volume fraction variation as a function of time for various *Mesh* sizes. The curves overlap, showing that the adopted meshes adequately could capture the melting phenome. However, reducing the mesh size below 75 resulted in convergence issues, which were avoided. Thus, the mesh size *Mesh*=75 was selected for the computations of the present research. A view of the adopted mesh is illustrated in Fig. 4.

3.3. Code verification

Considering the melting heat transfer in metal foams, the melting interface captured physically by Zheng et al. [17] was used as validation. In Fig. 5, the actual melting interface of copper foam - paraffin was compared with the simulation data of the current investigation. The simulations were executed for a uniform porous high porosity metal foam (97.5% porosity)

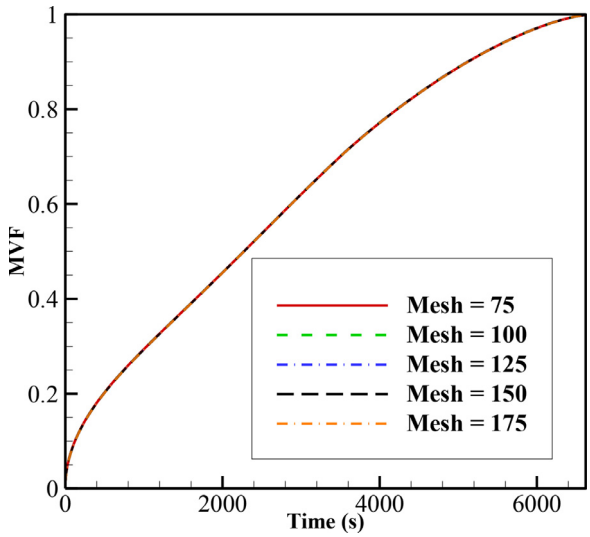

Fig. 3. The melting volume fraction for different mesh sizes.

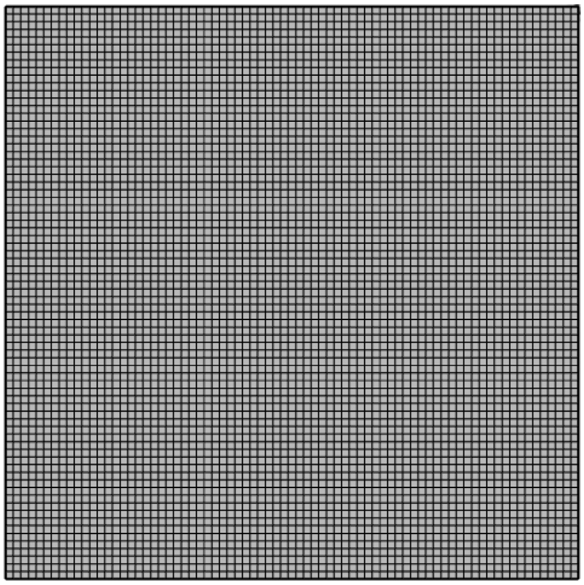

Fig. 4. A view of the selected mesh of size *Mesh*=75 for computations.

in a square enclosure of a height of 10 cm. The heat rate at the bottom wall was 1150 W/m^2. The enclosure was exposed to a heat source at the bottom. Fig. 5 demonstrates an agreement with the experimental images. There is a difference between the observed empirical melting interface and the computed melting interface for 3 h. The reason could be the formation of Rayleigh–Bénard cells for heating from below. These convection cells depend on the gap between the bottom wall and the melting interface; thus, their dynamic can change during the melting process. Thus, some differences between the melting interface shapes can be expected. However, the overall amount of molten PCM is similar for both empirical and simulated cases.

Considering the flow and heat transfer in a heterogenous porous medium, the results of the investigation of Fahs et al. [62] were utilized. They investigated the natural convection heat transfer in a cavity with a non-uniform permeability of $k(X, Y)$ and a non-uniformity coefficient ζ. Here, the non-dimensional temperature distribution (θ) reported by [62] and those of the present investigation are compared in Fig. 6. As seen, the results are in agreement with those of [62].

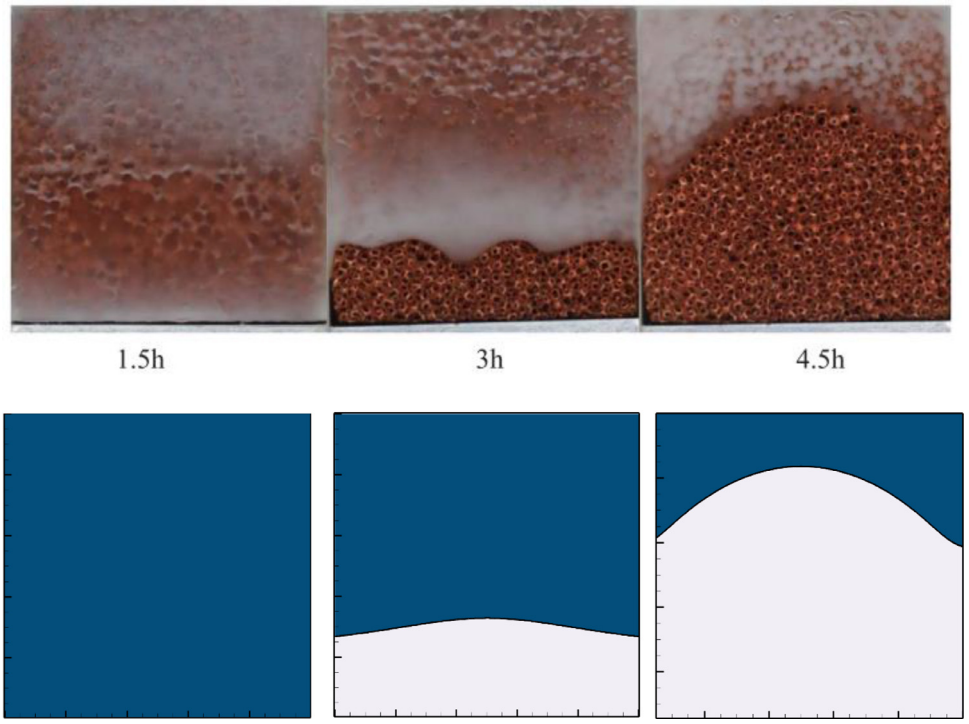

Fig. 5. The actual [17] and simulated melting interfaces for melting of paraffin wax in copper foam.

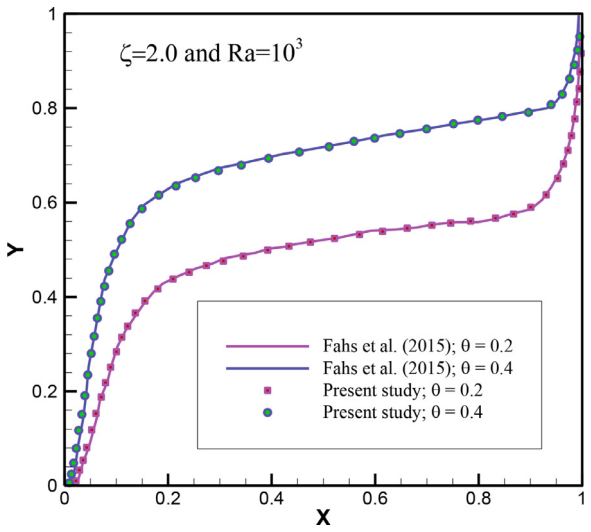

Fig. 6. The temperature distribution reported by [62] and those of present investigation.

4. Results and discussions

Fig. 7 depicts the influence of the heterogeneity parameter (δ) on the MVF and stored energy for a heterogeneity angle γ=45°. This figure shows the increase in heterogeneity could accelerate the melting process. The rate of thermal energy storage is also enhanced as heterogeneity increases. In the initial times, most of the cavity is filled with solid super cold PCM, and the conduction heat transfer is the dominant mechanism of heat transfer. In the initial times, the heterogeneity does not influence MVF notably since improving the conduction heat transfer in one direction would reduce the conduction heat transfer in the perpendicular direction. For the case of γ=45°, both perpendicular directions are almost natural to the heat transfer direction, and thus the change of δ results in a minimal impact on the MVF and heat transfer. It should be noted that at the initial times, there are no significant natural convection circulations; thus, the impact of δ on permeability

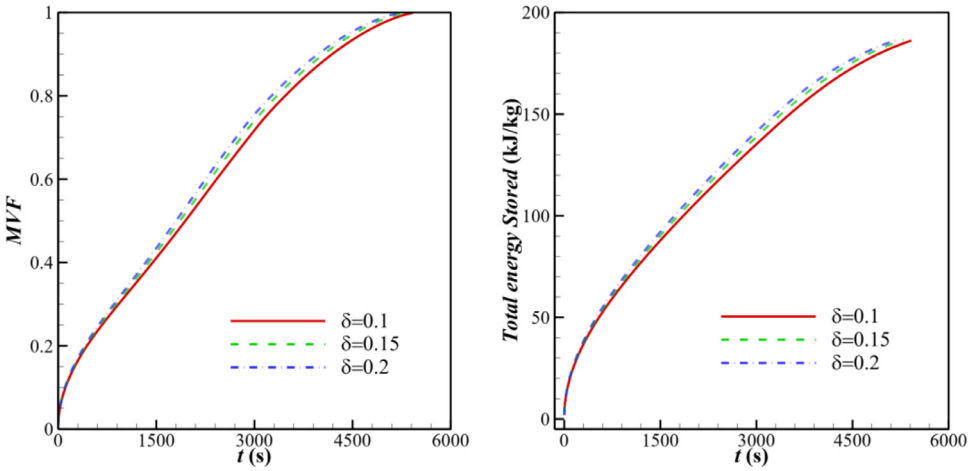

Fig. 7. Effect of δ on the melting volume fraction and total stored energy.

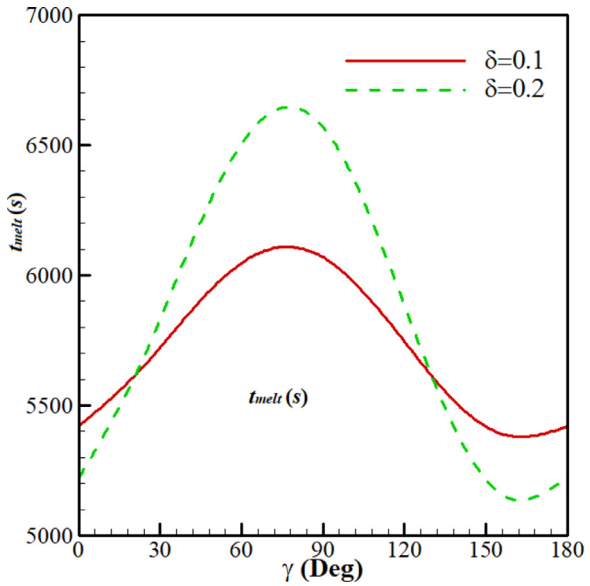

Fig. 8. Effect of angle on the melting time (t_{melt}).

and consequently on the convection heat transfer is minimal. After a while, the portion of liquid PCM increases, and natural convection flow forms. At this time, the permeability variation in perpendicular directions imposes a distinction between the MVF curves.

The heterogeneity angle was considered in the range of 0 to 180°. Fig. 8 is plotted to extensively investigate the impact of porous heterogeneity and its angle on the melting time. The results are reported for two cases of δ=0.1 and δ=0.2. A heterogeneity angle of 75° results in the longest melting time, which is about 6700s for δ=0.2. A heterogeneity angle of 0° provides a short melting time of about 5200 s which is 22% shorter than the case of γ=75°. The shortest melting time (5100 s) was obtained for γ=160° when δ=0.2. Thus, the variation of heterogeneity angle could change the melting time by about 24% when δ=0.2 and about 13% when δ=0.1.

Moreover, the full melting time for a case of simple (isotropic) metal foam (δ=0) was also computed as 5700 s. Using a metal foam (δ=0.2) with γ=75° increases the charging time by about 18% compared to the simple metal foam. However, using metal (δ=0.2) with γ=160° shortens the charging time by about 11% compared to a simple metal foam. Therefore, a heterogeneous metal foam could result in a shorter or longer melting time than a simple metal foam depending on the heterogeneity angle.

Figs. 9 and 10 show the isotherms and streamlines for various values of heterogeneity parameter (δ) at various time snapshots when γ=45°. These images show the melting front is more advanced for the case with higher heterogeneity parameters, particularly at the final times. This is since the most significant impact of the heterogeneity parameter is on

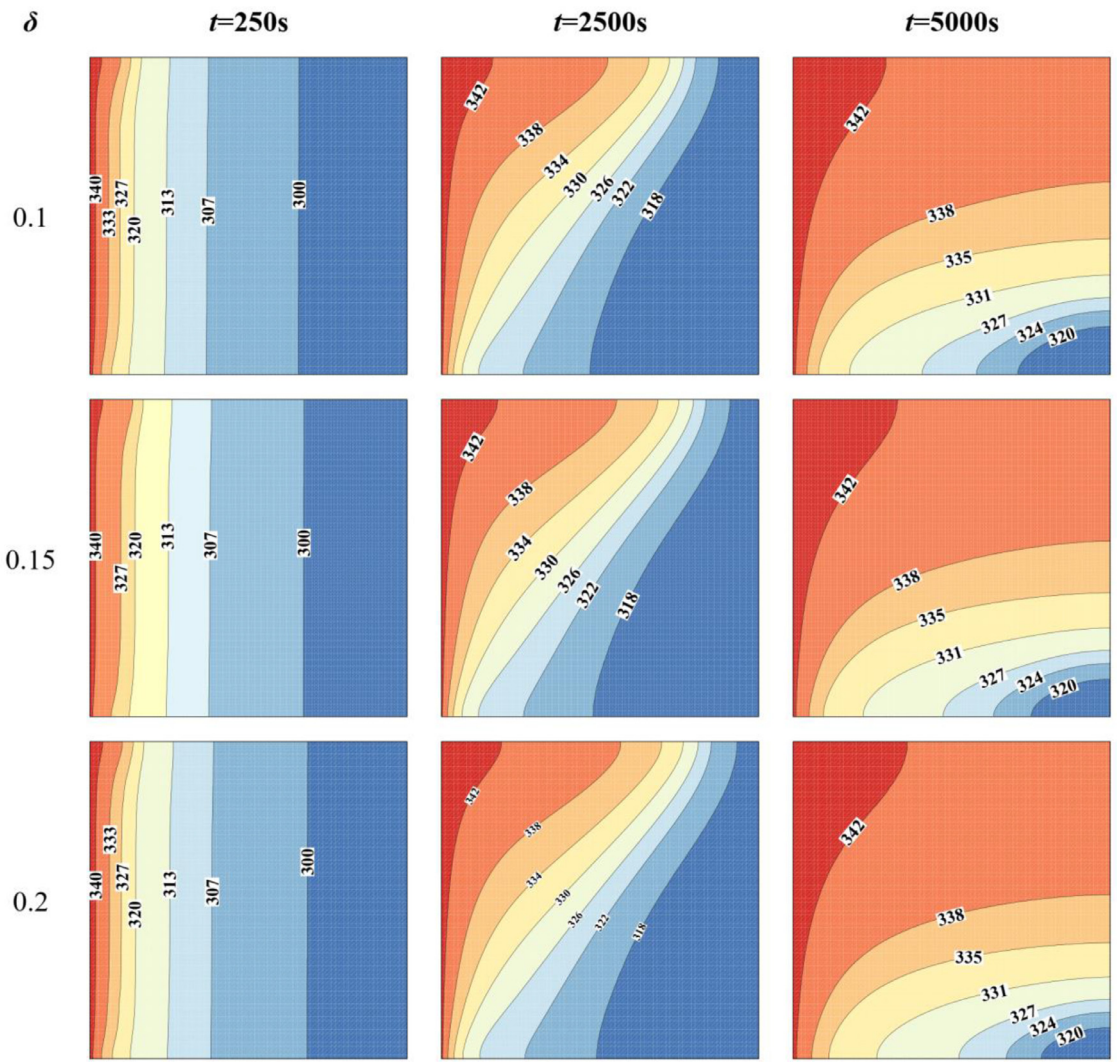

Fig. 9. The isotherms (K) at various time steps and values of heterogeneity parameter, top row: δ =0.1, middle row: δ =0.15 and bottom row: δ =0.2.

permeability. The permeability variation due to heterogeneity is important at the final stages of melting when the natural convection flows are strong. The influence of the heterogeneity parameter on isotherms is minimal and can be neglected.

Fig. 11 illustrates the influence of the heterogeneity angle on the characteristic parameters of MVF and total stored energy. The images are reported in two groups of $\gamma \leq 90°$ and $\gamma \geq 90°$ to avoid congestion. The results are reported for a case with δ=0.2. An increase of γ from zero to 90° decreases the MVF. The impact of γ on MVF is most significant at the final times, where most of the cavity is filled with liquid PCM, and the natural convection effects are important. Further increase of γ beyond 90° rises the MVF. Thus, the heterogeneity inclination angles of about 0° or 180° are the most advantageous angles to accelerate the melting process and reduce the thermal charging time. Considering Eq. (5), the thermal conductivity and permeability matrixes for both cases are similar. Thus, there is no theoretical distinction between the cases with heterogeneity inclination angles of 180° and 0°. Fig. 8 showed the optimum heterogeneity angle is 160°. The results of Fig. 11(b), also in agreement with the observation of Fig. 8, show the MVF curves are almost coincident for γ=157.5° and γ=180°, which is an indication of an optimum heterogeneity angle in this interval.

The energy storage curves show a similar trend of behavior as MVF when γ changes. This is because the amount of porosity and void space is fixed, and the variation of γ only changes the angle of heterogeneity in the domain. Here, the dominant mechanism of thermal energy storage is the latent heat thermal energy storage, which is directly related to the MVF. Thus, the variation trend of MVF and thermal energy storage is similar to γ changes.

Figs. 12 and 13 depict the isotherm and streamline for two values of heterogeneity angle (γ=0° and γ=90°) and various time snapshots when δ=0.2. As time advances, the melting front moves from the heated left vertical wall toward the right insulated wall. A comparison between the streamlines and melting front of two cases of γ=0° and γ=90° at t=2500s

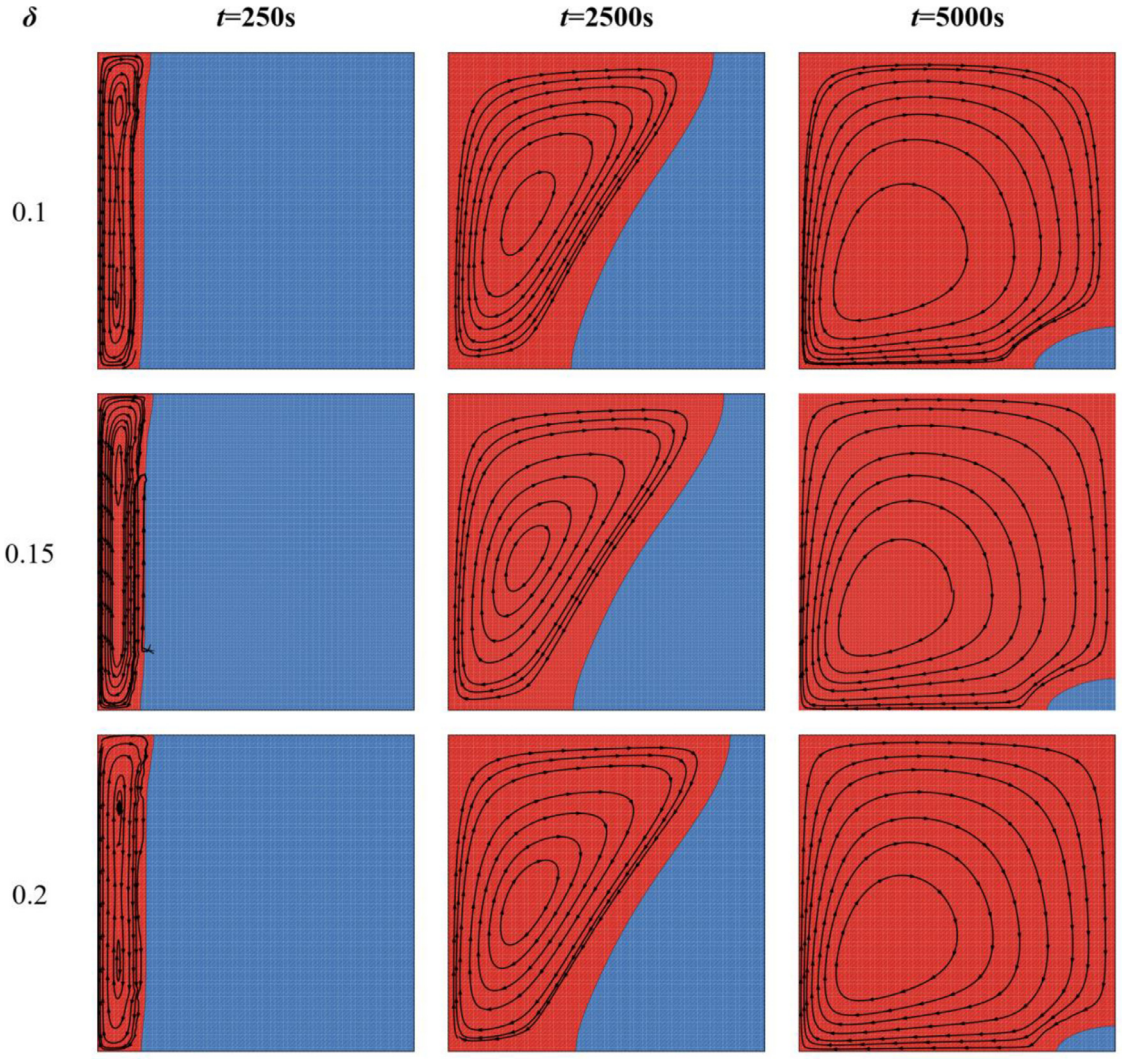

Fig. 10. The MVF and streamlines at various time steps and values of heterogeneity parameter, δ =0.1 (top row), δ =0.15 middle row, and δ =0.2 (bottom row).

indicates the melting front for the case γ=0° is more inclined to the right. There is also a wider top liquid region for case γ=0° compared to the case γ=90°. The reason for this behavior is hidden in the permeability and thermal conductivity matrixes.

Attention to Eq. (5) shows the permeability and thermal conductivity matrixes are:

$$\kappa_{mf@\gamma=0^\circ} = \begin{bmatrix} 0.8\kappa & 0 \\ 0 & 1.2\kappa \end{bmatrix} \textbf{ and } \quad k_{mf@\gamma=0^\circ} = \begin{bmatrix} 1.2k & 0 \\ 0 & 0.8k \end{bmatrix} \tag{13a}$$

Thus, as seen, the permeability in the *y*-direction is stronger than in the *x*-direction, while the thermal conductivity in the *x*-direction is stronger than in the y-direction when γ=0°. For the case of γ=90°, the permeability and thermal conductivity matrixes are obtained as:

$$\kappa_{mf@\gamma=90^\circ} = \begin{bmatrix} 1.2\kappa & 0 \\ 0 & 0.8\kappa \end{bmatrix} \textbf{ and } \quad k_{mf@\gamma=90^\circ} = \begin{bmatrix} 0.8k & 0 \\ 0 & 1.2k \end{bmatrix} \tag{13b}$$

As seen, a case with γ=0 could better direct the natural convection flows in the vertical direction and then diffuse the heat in the x-direction through the conduction heat transfer mechanism compared to a case with γ=90°. Thus, the melting front for the case γ=0° is more advanced than that of γ=90°. Fig. 12 also shows smaller temperature gradients in the x-direction for case γ=0° compared to that of γ=90°. This is since the *x* thermal conductivity for γ=0° is larger than that of γ=90°. However, it should be noted that the heat transfer in the x-direction is the product of the temperature gradient and

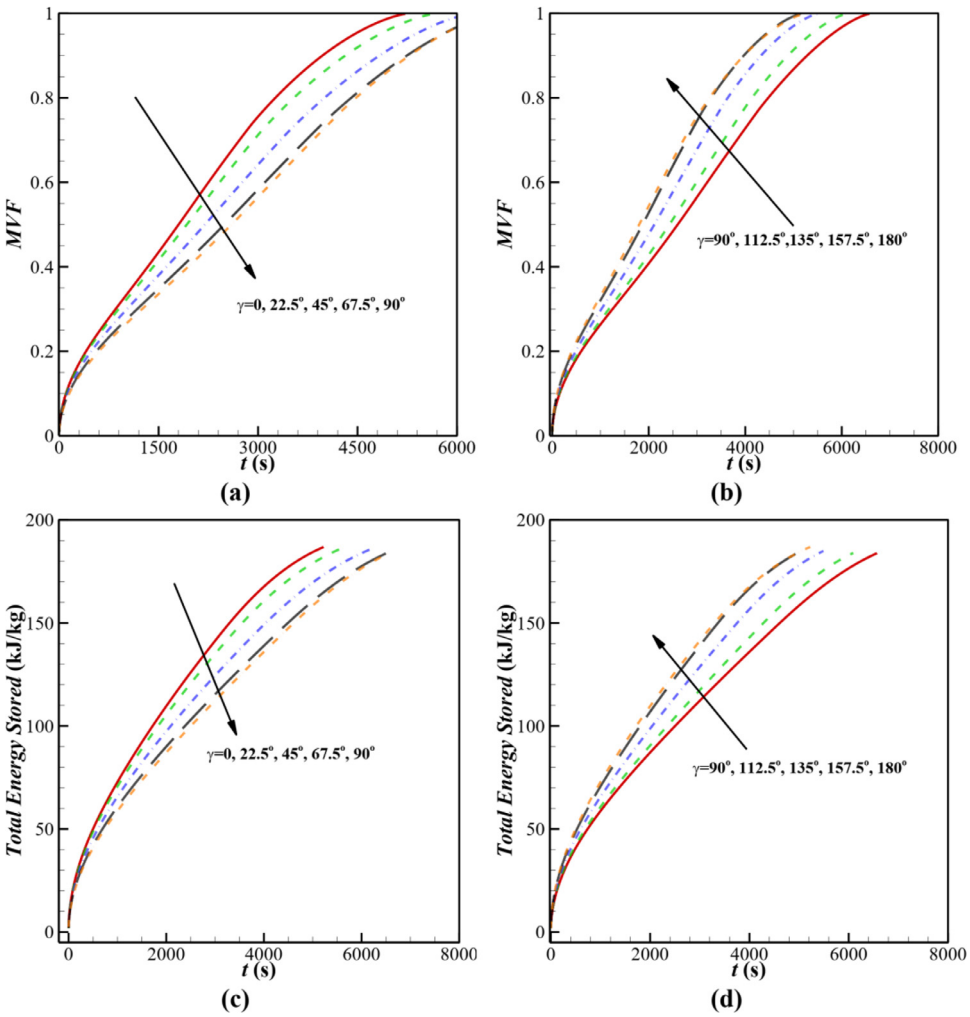

Fig. 11. Effect of γ on the melting volume fraction and total stored energy when δ=0.2.

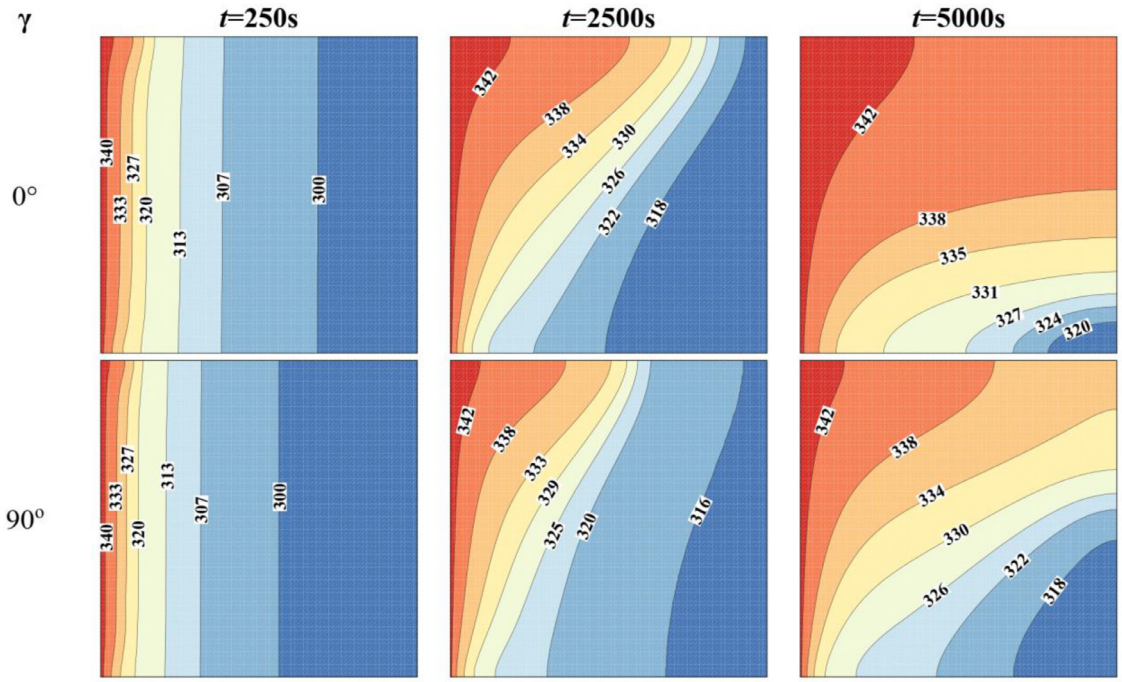

Fig. 12. Effect of inclination angle on the contours of isotherm (K) in δ=0.2

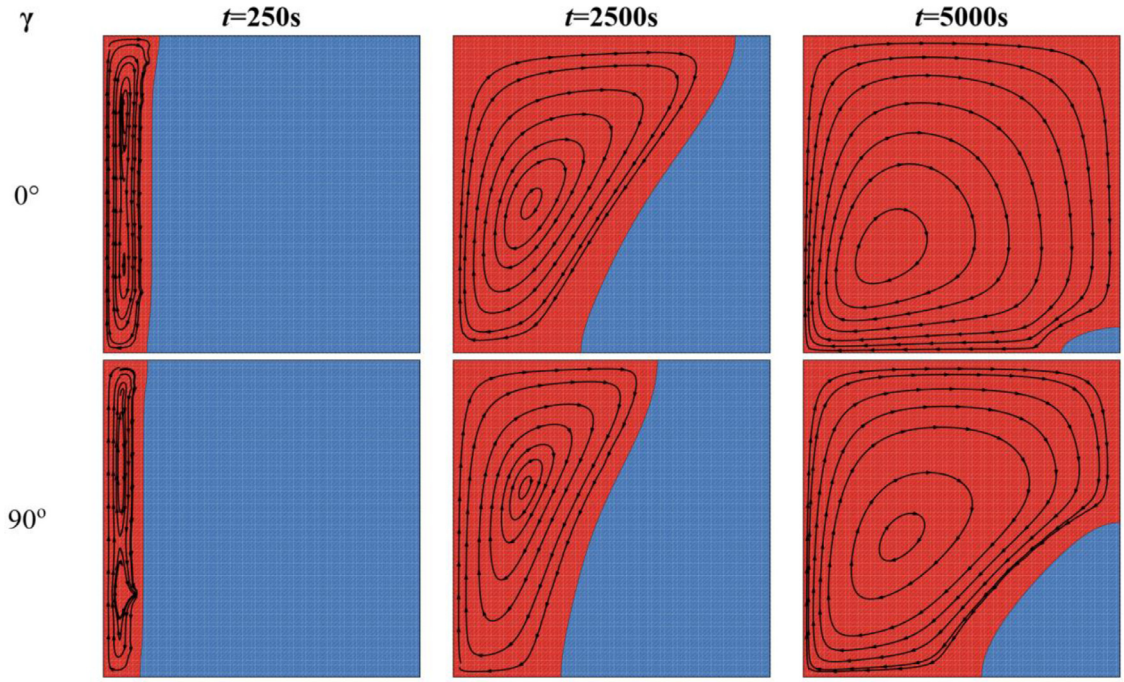

Fig. 13. The MVF and streamlines at various time steps and heterogeneity angle, when δ =0.2.

thermal conductivity. Although the x-temperature gradient for case γ=0° is small, the x-thermal conductivity is large, and hence, their product is large.

Moreover, the isotherm images show that the temperature gradients in the y-direction are generally smaller than in the x-direction. Thus, an increase of the thermal conductivity in the y-direction (as occurred in the case of γ=90°) cannot notably boost the heat transfer rate. Therefore, heterogeneity angle γ=0° much better accelerated the melting heat transfer compared to γ=90°.

6. Conclusion

Recently, metal foams with heterogeneous properties are promising candidates as thermal enhancers in latent heat thermal energy storage applications. The heterogeneous metal foams could show improved thermal conductivity or permeability in a specific direction. In the present study, the heterogeneous metal foams were modeled by specifying thermal conductivity and permeability tensors. Then, the governing equations for the conservation of mass, momentum, and energy were introduced as partial differential equations. The finite element method was employed to solve the equations in a cavity filled with a composite heterogeneous metal foam and PCM.

- The impact of a heterogeneity parameter and heterogeneity angle was addressed on the thermal charging time, thermal energy storage, and isotherms and streamlines. The results showed that the increase in heterogeneity parameter could reduce the melting time. Moreover, the heterogeneity angle could effectively change the melting time.
- A zero angled heterogeneity ($\gamma=0^\circ$) was a good candidate for the improvement of latent heat thermal energy storage since reinforcing the materials in the x-direction leads to the improved thermal conductivity in the x-direction and the improvement of permeability in the y-direction. Considering the dominant regime of heat transfer in the x-direction (heating from the vertical side wall), an improved permeability in the y-direction contributes to the natural convection flows. In contrast, an improved thermal conductivity in the x-direction boosts thermal diffusion. Thus, a case with $\gamma=0^\circ$ could reduce the melting time by 22% compared to a case with $\gamma=75^\circ$ when $\delta=0.2$.
- The variation of the heterogeneity angle can change the melting time by 13% when the heterogeneity parameter is just 0.1. For a higher heterogeneity parameter of $\delta=0.2$, the variation of the heterogeneity parameter can change the melting time by 24%. Depending on the heterogeneity angle. The thermal charging time can be increased by 18% or decreased by 11% compared to a simple metal foam.

Declaration of Competing Interest

The authors clarify that there is no conflict of interest for report.

CRediT authorship contribution statement

Mehdi Ghalambaz: Conceptualization, Methodology, Software, Validation, Formal analysis, Data curation. **Mutabe Aljaghtham:** Visualization, Writing – original draft, Investigation, Formal analysis, Data curation. **Ali J. Chamkha:** Visualization, Writing – original draft, Investigation, Formal analysis, Data curation. **Abdelkader Abdullah:** Methodology, Software, Formal analysis, Data curation. **Ibrahim Mansir:** Methodology, Software, Formal analysis, Data curation. **Mohammad Ghalambaz:** Investigation, Writing – review & editing, Supervision.

Data availability

No data was used for the research described in the article.

Acknowledgment

The authors extend their appreciation to the Deputyship for Research & Innovation, Ministry of Education in Saudi Arabia for funding this research work through the project number (IF-PSAU-2021/01/18928).

References

[1] G. Alva, Y. Lin, G. Fang, An overview of thermal energy storage systems, Energy 144 (2018) 341–378.
[2] Y. Huang, Z. Pang, Y. Kong, N. Watanabe, Assessment of the high-temperature aquifer thermal energy storage (HT-ATES) potential in naturally fractured geothermal reservoirs with a stochastic discrete fracture network model, J. Hydrol. 603 (2021) 127188.
[3] X. Yang, X. Wang, Z. Liu, X. Luo, J. Yan, Effect of fin number on the melting phase change in a horizontal finned shell-and-tube thermal energy storage unit, Solar Energy Mater. Solar Cells 236 (2022) 111527.
[4] Z.R. Li, G.T. Fu, L.W. Fan, Synergistic effects of nano-enhanced phase change material (NePCM) and fin shape on heat storage performance of a finned shell-and-tube unit: an experimental study, J. Energy Storage 45 (2022) 103772.
[5] J. Pássaro, A. Rebola, L. Coelho, J. Conde, G.A. Evangelakis, C. Prouskas, D.G. Papageorgiou, A. Zisopoulou, I.E. Lagaris, Effect of fins and nanoparticles in the discharge performance of PCM thermal storage system with a multi pass finned tube heat exchange, Appl. Therm. Eng. 212 (2022) 118569.
[6] J. Guo, Z. Liu, B. Yang, X. Yang, J. Yan, Melting assessment on the angled fin design for a novel latent heat thermal energy storage tube, Renew. Energy 183 (2022) 406–422.
[7] J. Guo, X. Wang, B. Yang, X. Yang, M.J. Li, Thermal assessment on solid-liquid energy storage tube packed with non-uniform angled fins, Solar Energy Mater. Solar Cells 236 (2022) 111526.
[8] Y. Zhang, M.V. Bozorg, J.F. Torres, Y. Zhao, X. Wang, Dynamic melting of encapsulated PCM in various geometries driven by natural convection of surrounding air: a modelling-based parametric study, J. Energy Storage 48 (2022) 103975.
[9] M.Y. Yazici, M. Saglam, O. Aydin, M. Avci, Thermal energy storage performance of PCM/graphite matrix composite in a tube-in-shell geometry, Therm. Sci. Eng. Prog. 23 (2021).
[10] M.M. Heyhat, S. Mousavi, M. Siavashi, Battery thermal management with thermal energy storage composites of PCM, metal foam, fin and nanoparticle, J. Energy Storage 28 (2020).
[11] X. Li, H. Li, X. Kong, H. Yang, Characterization and experimental investigation of composite phase change materials based on aluminum nitride/expanded graphite, J. Energy Storage 35 (2021) 102326.

[12] A. Andreozzi, N. Bianco, M. Iasiello, V. Naso, Thermo-fluid-dynamics of a ceramic foam solar receiver: a parametric analysis, Heat Transf. Eng. 41 (2019) 1085–1099.
[13] N. Bianco, M. Iasiello, G.M. Mauro, L. Pagano, Multi-objective optimization of finned metal foam heat sinks: tradeoff between heat transfer and pressure drop, Appl. Therm. Eng. 182 (2021) 116058.
[14] X. Yang, P. Wei, X. Wang, Y.L. He, Gradient design of pore parameters on the melting process in a thermal energy storage unit filled with open-cell metal foam, Appl. Energy 268 (2020) 115019.
[15] S.N. J, Ercan Mehmet DEDE, Thermal Management Systems Including Multiple Phase Changing Materials and Vehicles Including the Same, Toyota Motor Engineering & Manufacturing North America, Inc, Plano, TXUnited States, 2018 (US).
[16] C. Nie, J. Liu, S. Deng, Effect of geometry modification on the thermal response of composite metal foam/phase change material for thermal energy storage, Int. J. Heat Mass Transf. 165 (2021) 120652.
[17] H. Zheng, C. Wang, Q. Liu, Z. Tian, X. Fan, Thermal performance of copper foam/paraffin composite phase change material, Energy Convers. Manag. 157 (2018) 372–381.
[18] S.K. Razack, K. Razack, S. Ali, Thermal Management System and Device, European Patent Office, 2020.
[19] J. Guo, Z. Du, G. Liu, X. Yang, M.J. Li, Compression effect of metal foam on melting phase change in a shell-and-tube unit, Appl. Therm. Eng. 206 (2022) 118124.
[20] G. Liu, T. Xiao, J. Guo, P. Wei, X. Yang, K. Hooman, Melting and solidification of phase change materials in metal foam filled thermal energy storage tank: evaluation on gradient in pore structure, Appl. Therm. Eng. 212 (2022) 118564.
[21] Z. Deng, X. Liu, C. Zhang, Y. Huang, Y. Chen, Melting behaviors of PCM in porous metal foam characterized by fractal geometry, Int. J. Heat Mass Transf. 113 (2017) 1031–1042.
[22] H. Xu, F. Yao, C. Zhang, Numerical study on melting heat transfer in fractal metal foam, Fractals 27 (2019) 1950106.
[23] R. Sabrina Ferfera, B. Madani, R. Serhane, Investigation of heat transfer improvement at idealized microcellular scale for metal foam incorporated with paraffin, Int. J. Therm. Sci. 156 (2020) 106444.
[24] R. Tauseef ur, H.M. Ali, M.M. Janjua, U. Sajjad, W.M. Yan, A critical review on heat transfer augmentation of phase change materials embedded with porous materials/foams, Int. J. Heat Mass Transf. 135 (2019) 649–673.
[25] S. Filippeschi, M. Mameli, P. Di Marco, Experimental analysis of the melting process in a PCM/aluminum foam composite material in hypergravity conditions, Interfacial Phenom. Heat Transf. 6 (2018) 451–467.
[26] X. Hu, F. Zhu, X. Gong, Numerical investigation of the effects of heating and contact conditions on the thermal charging performance of composite phase change material, J. Energy Storage 30 (2020) 101444.
[27] X. Yang, Z. Guo, Y. Liu, L. Jin, Y.L. He, Effect of inclination on the thermal response of composite phase change materials for thermal energy storage, Appl. Energy 238 (2019) 22–33.
[28] C. Prieto, A. Lopez-Roman, N. Martínez, J.M. Morera, L.F. Cabeza, Improvement of Phase Change Materials (PCM) used for solar process heat applications, Molecules 26 (2021) 1260.
[29] S. Du, T. Xia, Y.L. He, Z.Y. Li, D. Li, X.Q. Xie, Experiment and optimization study on the radial graded porous volumetric solar receiver matching non-uniform solar flux distribution, Appl. Energy 275 (2020) 115343.
[30] E. Rezaei, M. Barbato, S. Gianella, A. Ortona, S. Haussener, Pressure drop and convective heat transfer in different SiSiC structures fabricated by indirect additive manufacturing, J. Heat Transf. 142 (2020) 032702.
[31] Z.B. Li, X.Y. Li, Y.X. Zheng, Biaxial mechanical behavior of closed-cell aluminum foam under combined shear—compression loading, Trans. Nonferrous Metals Soc. China 30 (2020) 41–50.
[32] F. Zhu, C. Zhang, X. Gong, Numerical analysis on the energy storage efficiency of phase change material embedded in finned metal foam with graded porosity, Appl. Therm. Eng. 123 (2017) 256–265.
[33] V. Joshi, M.K. Rathod, Thermal performance augmentation of metal foam infused phase change material using a partial filling strategy: an evaluation for fill height ratio and porosity, Appl. Energy 253 (2019) 113621.
[34] J.M. Mahdi, E.C. Nsofor, Multiple-segment metal foam application in the shell-and-tube PCM thermal energy storage system, J. Energy Storage 20 (2018) 529–541.
[35] J.M. Mahdi, H.I. Mohammed, E.T. Hashim, P. Talebizadehsardari, E.C. Nsofor, Solidification enhancement with multiple PCMs, cascaded metal foam and nanoparticles in the shell-and-tube energy storage system, Appl. Energy 257 (2020) 113993.
[36] Y. Xu, M.J. Li, Z.J. Zheng, X.D. Xue, Melting performance enhancement of phase change material by a limited amount of metal foam: configurational optimization and economic assessment, Appl. Energy 212 (2018) 868–880.
[37] M. Iasiello, N. Bianco, W.K.S. Chiu, V. Naso, Thermal conduction in open-cell metal foams: anisotropy and representative volume element, Int. J. Therm. Sci. 137 (2019) 399–409.
[38] M. Iasiello, N. Bianco, W.K.S. Chiu, V. Naso, Anisotropic convective heat transfer in open-cell metal foams: assessment and correlations, Int. J. Heat Mass Transf. 154 (2020) 119682.
[39] M. Iasiello, M. Mameli, S. Filippeschi, N. Bianco, Metal foam/PCM melting evolution analysis: orientation and morphology effects, Appl. Therm. Eng. 187 (2021) 116572.
[40] Y. Amani, A. Takahashi, P. Chantrenne, S. Maruyama, S. Dancette, E. Maire, Thermal conductivity of highly porous metal foams: experimental and image based finite element analysis, Int. J. Heat Mass Transf. 122 (2018) 1–10.
[41] D. Vijay, P. Goetze, R. Wulf, U. Gross, Homogenized and pore-scale analyses of forced convection through open cell foams, Int. J. Heat Mass Transf. 123 (2018) 787–804.
[42] J. Yang, L. Yang, C. Xu, X. Du, Numerical analysis on thermal behavior of solid–liquid phase change within copper foam with varying porosity, Int. J. Heat Mass Transf. 84 (2015) 1008–1018.
[43] X. Huang, C. Sun, Z. Chen, Y. Han, Experimental and numerical studies on melting process of phase change materials (PCMs) embedded in open-cells metal foams, Int. J. Therm. Sci. 170 (2021) 107151.
[44] M.A. Bamdezh, G.R. Molaeimanesh, S. Zanganeh, Role of foam anisotropy used in the phase-change composite material for the hybrid thermal management system of lithium-ion battery, J. Energy Storage 32 (2020) 101778.
[45] P. Yu, Y. Wang, R. Ji, H. Wang, J. Bai, Pore-scale numerical study of flow characteristics in anisotropic metal foam with actual skeleton structure, Int. Commun. Heat Mass Transf. 126 (2021) 105401.
[46] Q. Ren, Z. Wang, T. Lai, J.F. Zhang, Z.G. Qu, Conjugate heat transfer in anisotropic woven metal fiber-phase change material composite, Appl. Therm. Eng. 189 (2021) 116618.
[47] M. Iasiello, M. Mameli, S. Filippeschi, N. Bianco, Metal foam/PCM melting evolution analysis: orientation and morphology effects, Appl. Therm. Eng. 187 (2021) 116572.
[48] P. Zhang, Z. Meng, H. Zhu, Y. Wang, S. Peng, Melting heat transfer characteristics of a composite phase change material fabricated by paraffin and metal foam, Appl. Energy 185 (2017) 1971–1983.
[49] A.A. Nnanna, A. Haji-Sheikh, K.T. Harris, Experimental study of local thermal non-equilibrium phenomena during phase change in porous media, Int. J. Heat Mass Transf. 47 (2004) 4365–4375.
[50] K. Jiao, L. Lu, T. Wen, Q. Wang, A modified mixture theory for one-dimensional melting of pure PCM and PCM/metal foam composite: numerical analysis and experiment validation, Int. J. Heat Mass Transf. 186 (2022) 122461.
[51] X. Hu, X. Gong, Pore-scale numerical simulation of the thermal performance for phase change material embedded in metal foam with cubic periodic cell structure, Appl. Therm. Eng. 151 (2019) 231–239.

[52] J.M. Mahdi, H.I. Mohammed, E.T. Hashim, P. Talebizadehsardari, E.C. Nsofor, Solidification enhancement with multiple PCMs, cascaded metal foam and nanoparticles in the shell-and-tube energy storage system, Appl. Energy 257 (2020) 113993.
[53] S.M.H. Zadeh, S. Mehryan, M. Ghalambaz, M. Ghodrat, J. Young, A. Chamkha, Hybrid thermal performance enhancement of a circular latent heat storage system by utilizing partially filled copper foam and Cu/GO nano-additives, Energy 213 (2020) 118761.
[54] X.H. Yang, J.X. Bai, H.B. Yan, J.J. Kuang, T.J. Lu, T. Kim, An analytical unit cell model for the effective thermal conductivity of high porosity open-cell metal foams, Transp. Porous Media 102 (2014) 403–426.
[55] X. Yang, J. Kuang, T. Lu, F. Han, T. Kim, A simplistic analytical unit cell based model for the effective thermal conductivity of high porosity open-cell metal foams, J. Phys. D Appl Phys. 46 (2013) 255302.
[56] A. Bhattacharya, V.V. Calmidi, R.L. Mahajan, Thermophysical properties of high porosity metal foams, Int. J. Heat Mass Transf. 45 (2002) 1017–1031.
[57] X. Xiao, P. Zhang, M. Li, Preparation and thermal characterization of paraffin/metal foam composite phase change material, Appl. Energy 112 (2013) 1357–1366.
[58] X. Yang, T.J. Lu, T. Kim, An analytical model for permeability of isotropic porous media, Phys. Lett. A 378 (2014) 2308–2311.
[59] D.A. Nield, A. Bejan, Convection in Porous Media, Springer, 2006.
[60] O.C. Zienkiewicz, R.L. Taylor, P. Nithiarasu, The Finite Element Method for Fluid Dynamics, Seventh Edition ed., Butterworth-Heinemann, Oxford, 2014.
[61] G. Söderlind, L. Wang, Adaptive time-stepping and computational stability, J. Comput. Appl. Math. 185 (2006) 225–243.
[62] M. Fahs, A. Younes, A. Makradi, A reference benchmark solution for free convection in a square cavity filled with a heterogeneous porous medium, Numer. Heat Transf. Part B Fundam. 67 (2015) 437–462.